PHOTOCATALYTIC CONVERSION OF CO₂ INTO RENEWABLE FUELS: MATERIAL AND REACTOR DESIGN

Van-Huy Nguyen*

Institute of Research and Development, Duy Tan University, Da Nang 550000, Vietnam
Supporting Information

ABSTRACT. Photocatalytic conversion of CO_2 by using sustainable sunlight energy to convert CO_2 greenhouse gas to renewable fuels has received increasing interest. This idea could simultaneously solve both problems of global warming and sustainable energy shortage. Several types of photocatalyst material and reactor for photocatalytic CO_2 reduction for realizing solar fuels have been developed extensively. Emphasis is given to both TiO_2-based and non-TiO_2-based materials. Among photocatalysts, salt composites and zeolitic imidazolate frameworks, which are economical material, have exhibited outstanding photocatalytic efficiencies. For the reactor, an internally illuminated monolith reactor has performed an excellent photocatalytic activity. The critical challenges, prospects and the need to give more attention to the design of photocatalyst and reactor for solar energy conversion of CO_2 into renewable fuels have been highlighted successfully.

KEYWORDS: *reactor, photocatalyst material, renewable fuel, photocatalytic conversion, carbon dioxide (CO_2)*

1. INTRODUCTION

Nowadays, warming of climate change and energy shortage are some of the most significant challenges for humanity [1]. On the one hand, carbon dioxide (CO_2) and other key greenhouse gases (methane, nitrous oxide, and fluorinated gases), which are accumulating in Earth's atmosphere, has been linked to climate change. On the other hand, the energy shortage is also a global issue since the capacity of fossil fuels could not cover the ongoing expansion of the world energy demand. Noting that excessive use of fossil fuels is also considered as a critical cause of global climate change. Therefore, there is an urgent need for finding alternative energy sources for sustainable economic growth [2].

There is a growing interest in the use of CO_2 as the most abundant and economic carbon-containing sources for the development of alternative energy [3]. Typically, the CO_2 utilization processes are classified into four groups (as seen in Table 1), including biocatalytic [4-6], catalytic [7-10], photocatalytic [11-14] and electrocatalytic [15, 16] processes. The idea to drive photocatalytic reactions by using renewable solar energy for converting CO_2 waste gas pollution into substitute fuels provides a viable solution. This promising approach not only reduces CO_2 emission but also simultaneously recycles it as renewable fuel by harvesting readily available solar energy. Among many factors, the presence of efficient photocatalysts plays an essential role in determining the photocatalytic efficiency. On the other approach, enhancing of light harvesting, reducing of photon losses and charge carrier recombination have received attention for the design of a more effective reactor [17, 18].

Herein, we review the research advances made in the design and development of photocatalyst material, and reactor for photocatalytic conversion of CO_2. Different types of photocatalyst, reactor configurations affecting the yield and distribution of products are discussed.

2. PHOTOCATALYST MATERIAL

One of the most significant approach to improve efficiency is to develop and design new photocatalyst. Emphasis is given to TiO_2-based materials with many advantages, such as cheap, nontoxic, chemical stability, and resistant to photo-corrosion [19]. However, the TiO_2 properties, such as relatively large band-gap energy and rapid electron-hole recombination, should be improved. Hence, to utilize solar radiation for photo-conversion of CO_2, two approaches have been employed as follows:

2.1. Modified TiO₂-based materials

Several methods to develop visible light response TiO_2 photocatalysts, including cation doping (Fe, Co, Ni, Mn, V, Cu, and Zn, etc.), anion doping (carbon (C), boron (B), Sulphur (S) and nitrogen (N)), semiconductors coupling (CdS, Cu_2O, $FeTiO_3$ and $CuFe_2O_4$, etc.), and surface alkali/base modification, are proposed and summarized in Table 2 [20-29]. As expected, modified TiO_2, compared with pristine TiO_2, shows a better absorb photons ability in the visible region and a lower rate of electron-hole recombination, resulting in achieving better photocatalytic performance. In/TiO_2 performs the best photocatalytic activity (up to 578 $\mu mol \cdot g_{cat}^{-1} \cdot h^{-1}$ of CH_4) [20]. N_2H_4/TiO_2 could achieve 416 $\mu mol \cdot g_{cat}^{-1} \cdot h^{-1}$ of CH_3OH [28]. Recent approaches using five surface modification methods for enhancing photocatalytic CO_2 reduction performance of TiO_2, including impurity doping, metal deposition, alkali modification, heterojunction construction, and carbon-based material loading, are also reviewed [30]. Each of these techniques has its advantages and disadvantages; hence, to combine different modification methods might be a good idea to balance the advantages and disadvantages, resulting in developing more efficient TiO_2-based photocatalysts.

2.2. Non-TiO₂ based materials

Non-TiO_2 based photocatalysts are categorized into three groups depending on their structure/chemical nature [31]. The first category includes single-metal oxides, mixed-metal oxides, metal oxide composites, layered double hydroxides (LDHs) and salt composites. The second category (carbon-based semiconductors) consists of graphene-based composites, carbon nanotube (CNT) composites, g-C_3N_4 composites. Lately, a third category that of hybrid organic-inorganic photocatalytic materials - Zeolitic imidazolate frameworks (ZIFs). Among carbonaceous hybrids, hexamolybdate clusters $Cs_2Mo_6Bri_8Bra_6/GO$) exhibit the

best photocatalytic activity (up to 69 μmol·g$_{cat}^{-1}$·h^{-1} of CH_3OH) [32]. Single-metal oxides, mixed-metal oxides, and metal oxide composites could produce up to 170 μmol·g$_{cat}^{-1}$·h^{-1} of CH_3OH by Ni [33]. LDHs performs a slightly higher photocatalytic activity, up to 210 μmol·g$_{cat}^{-1}$·h^{-1} of CH_3OH by Cu-Ni-Al LDH [34]. ZIFs could achieve 342 μmol·g$_{cat}^{-1}$·h^{-1} of CH_3OH by orthorhombic copper (II) imidazolate frameworks [35]. Importantly, salt composites exhibit excellent photocatalytic activity (up to 526 μmol·g$_{cat}^{-1}$·h^{-1} of $C_2H_4O_2$ (methyl formate)) by cubic $CdIn_2S_4$ microspheres [36].

Among photocatalysts, salt composites and ZIFs, which are economical materials, have exhibited outstanding photocatalytic efficiencies. However, the derived photo-efficiency is still relatively low and its comparative impracticality for commercial applications. In addition to an efficient semiconductor photocatalyst for increasing the effectiveness of photocatalytic performance, designing and developing a new reactor for the photo-reduction of CO_2 would be beneficial.

3. REACTOR DESIGN

The reactor is integral to the photocatalysis process and constitutes a vital engineering factor. Some key parameters determine the types of reactor, such as the phases involved (single phase (gas, liquid), multiphase (gas-liquid, gas-solid, liquid-solid, gas-liquid-solid)), the mode of hydrodynamic operation (batch, semi-batch, or continuous), the mixing and flow characteristics (completely mixed, some back-mixing, plug flow, non-ideal flow characteristics), the geometric configuration (dimensions and shape), the light source specifications (output power, spectral distribution, shape, dimensions, operating and maintenance requirements), and the radiation source configuration relative to the reaction space [37, 38]. Several reactor types for photocatalytic conversion of CO_2 to produce solar fuels are summarized in Table 3 [39-54].

3.1. Slurry reactor

First, a slurry reactor with a suspended catalyst has been employed extensively for CO_2 photo-reduction [39-42]. These fundamental studies aimed to either derives kinetic data or design a large reactor. This type of reactor offers many advantages such as (1) a simple construction and a lower investment for a large-scale reactor, (2) the possibility for a large-capacity design, and (3) the low amount of photocatalyst used. Very early, Inoue et al. reported the photocatalytic reduction of CO_2 in a glass cell [39]. Fujiwara et al. experimented with a closed pyrex tube (8 mm in diameter) [40]. Similarly, Grodkowski and Neta used a pyrex bulb (43 mL in volume) [41]. Lu et al. experimented with a 358-mL cylindrical glass vessel [42]. Lee et al. used a tubular glass reactor [55]. Yang et al. designed a stirred-batch annular quartz reactor, as shown in Figure 1 [43]. This reactor could be used as an aqueous NaOH solution with continuous CO_2 bubble flow under light irradiation. Wu et al. conducted a photocatalytic reaction in a slurry batch reactor under saturated CO_2 absorption [44]. However, it notes that slurry-type reactor has many disadvantages including the separation of photocatalyst particles from the reaction mixture, low possibility of photocatalyst recycling, inefficient distribution of light throughout the system, and the challenge of product separation.
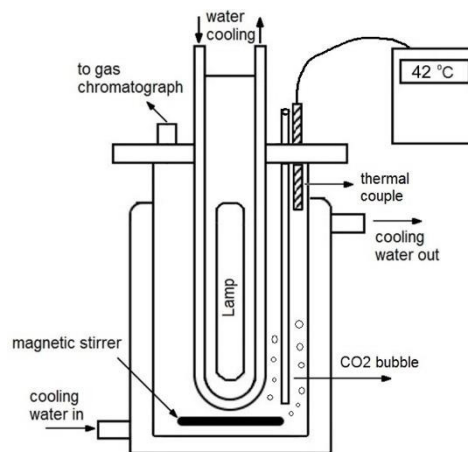

Figure 1. *Schematic of a stirred batch annular quartz reactor. (Reprinted from H.-C. Yang et al./ Catal. Lett. (2009) 131: 381)*
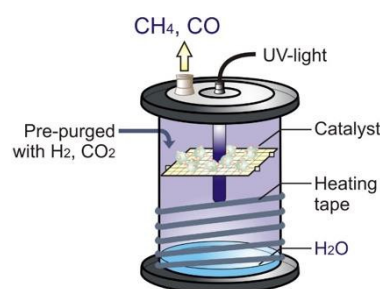
3.2. Fixed-bed reactor

Figure 2. *Schematic of a pyrex single reactor system. (Reprinted from B.-R. Chen et al./ Phys. Chem. Chem. Phys., 2016,18, 4942–4951)*

The fixed-bed reactor has various advantages over traditional slurry reactors, such as (1) a higher throughput because of the higher gas velocity and (2) the possibility to immobilize catalysts onto fixed supports, thereby avoiding the drawback of catalyst separation [45-47]. A closed-circulation gas reactor, proposed by Yamagata et al., was also considered for CO_2 photo-reduction [45]. A disc of foam glass, placed inside the reactor, was used to load the photocatalyst. Zhang et al. also designed a fixed-bed reactor for the photo-reduction of CO_2 using a Pt/TiO_2 photocatalyst [46]. A flat quartz glass plate was integrated into the tube to hold the photocatalyst. The reactor (265 mL) measured 400 mm (length) × 35 mm (outside diameter). In another study, Tan et al. developed a new fixed-bed photocatalytic reactor [47]. A cylindrical quartz tube reactor was integrated with a flat glass tray to hold the catalysts. The reactor measured 300 mm (length) × 74 mm (outside diameter) × 3.0 mm (thickness). Moreover, Lo et al. designed a circulated reactor that could provide a fairly high specific surface area and uniform gas concentrations inside the reactor [48]. This reactor was made from a quartz tube with a length of 480 mm and an internal diameter of 22.5 mm. Pyrex glass pellets (3.0 mm in diameter) pre-immobilized with a powder photocatalyst were packed inside the reactor. Recently, a single pyrex reactor (385 mL in volume) was designed for the photocatalytic hydrogenation of CO_2 with H_2O (Figure 2) [49]. A flat teflon surface fixed in the middle of the reactor was used to place the photocatalyst powder evenly.

In another study, the design of a reactor for more efficient photo hydrogenation of CO_2 was addressed by comparing three types of reactors: a gas-phase reactor, a liquid-phase reactor, and a gas-liquid-phase reactor [56]. In the gas-phase

system, a cylindrical tube reactor (pyrex, 260 mL) was used with a quartz plate (92 mm × 40 mm × 2 mm) to pack the photocatalyst. For the liquid-phase system (pyrex, 385 mL), the photocatalyst was suspended in the liquid phase by stirring. The gas-liquid-phase system was very similar to the liquid-phase system and was combined with a teflon plate. The highest quantum efficiency was achieved using the gas-liquid-phase reactor (1.1×10^{-3} %), whereas the efficiency levels of the gas- and liquid-phase systems were only 0.1×10^{-3} % and 0.5×10^{-3} %, respectively. Both H_2 in the gas phase and the proton in the liquid phase could be utilized simultaneously, which contributed to the efficiency enhancement. However, the overall efficiency of the reaction was still very low. A low surface-to-volume ratio and an inefficient light distribution due to the geometry of the light source and the distance between the light source and the photocatalysts resulted in poor interaction between the reactants and the photocatalyst. The above-mentioned is the main issue for this type of reactor [57].

3.2.1. Optical-fiber reactor

In another approach, researchers improved the transmission and distribution of light energy. A first optical-fiber reactor was introduced by Hofstadlert and Bauer for photocatalytic wastewater treatment using TiO_2 immobilized on fused-silica glass fibers [58]. The reactor comprised many fibers serving as a medium to effectively and uniformly deliver light to the photocatalyst surface. An optical-fiber reactor has been successfully used for the photocatalytic reduction of CO_2 in a steady-state flow system [13, 50, 51, 59-62]. Figure 3 presents a schematic and a photograph of an optical-fiber reactor (216 mL in volume) with 216 catalyst-coated optical fibers (110 mm in length) [50].
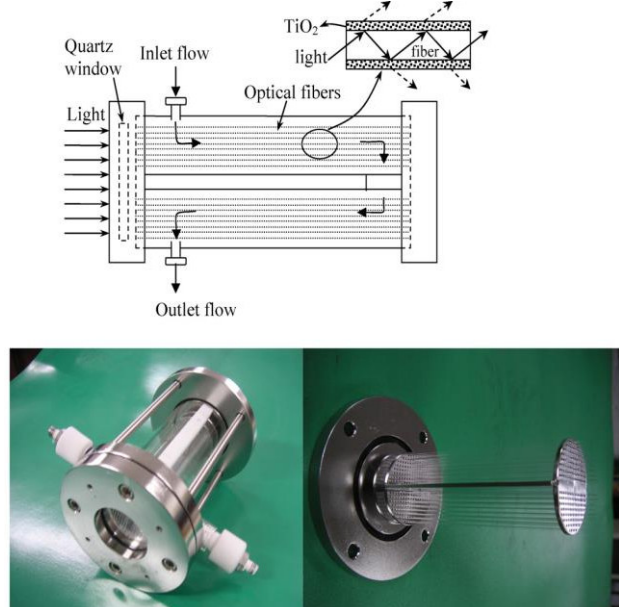

Figure 3. Schematic and a digital photograph of an optical-fiber reactor. (Reprinted from T.-V. Nguyen, J.C.S. Wu/ Appl. Catal. A 335 (2008) 112–120)

The photocatalyst-coated optical fibers were assembled in the reactor so that the light source could enter along the fibers

to induce the photocatalytic reaction on its surface. Notably, the transformation of CO_2 to hydrocarbons using sunlight is one of the best routes to producing renewable energy. Nguyen et al. synthesized a metal-doped TiO_2 catalyst sensitized with RuII(2,2′-bipyridyl-4,4′-dicarboxylate)2-(NCS)$_2$ (N3 dye), which was employed to photo-reduce CO_2 with H_2O under concentrated natural sunlight in an optical-fiber reactor [51]. The optical-fiber reactor provides a medium to transmit light uniformly throughout the reactor, compared with a traditional packed-bed reactor and consequently increases the photo-conversion efficiency. However, one of the disadvantages to this type of reactor is that it does not effectively utilize the entire reactor volume. Because a photocatalyst is coated on optical fibers that are usually thin and constitute only 20-30 % of the reactor volume, it provides a relatively low surface area for the coating support.

3.2.2. Monolith reactor

To solve the mentioned concerns, a monolith reactor which provides (1) a large ratio of illuminated surface area to reactor volume and (2) efficient light utilization/ distribution over the photocatalyst surface, could be advantageous. The specific surface area of a monolith (also called honeycomb) is 10-100 times higher than that of other types of catalyst support [63]. Various photocatalysts are prepared to load the monolith channels by using sol-gel dip-coating methods, including N/TiO_2 and Cu/TiO_2 [64], Cu-In/TiO_2 [65], In/TiO_2 [52], $NiO/InTaO_4$ [53], Pd/TiO_2 and Rh/TiO_2 [54], Mn/TiO_2 [66], and Ag/TiO_2 [67]. Recently, a monolith reactor comprising a stainless steel cylindrical vessel (5.5 cm in length, 150 mL in volume) was designed, as illustrated in Figure 4 [52]. The quantum efficiency of this monolith reactor was 200 times higher than that of a cell-type reactor. The significant improvement in the monolith reactor was attributed to a higher illuminated surface area, higher photon energy consumption, and better reactor volume utilization, compared with a cell-type reactor.
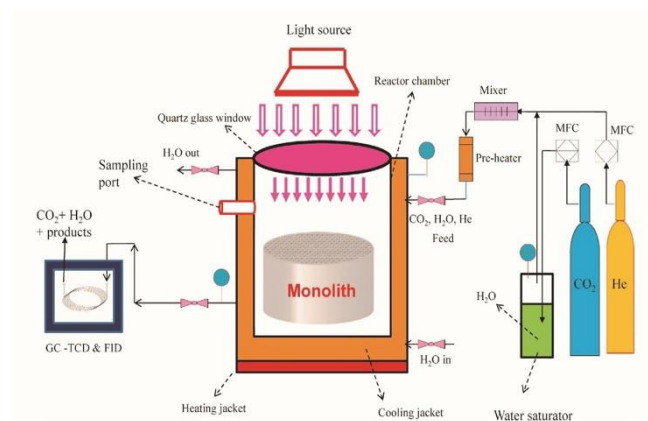

Figure 4. Schematic of an experimental setup using a monolith reactor. (Reprinted from M. Tahir and N.-S. Amin/ Appl. Catal. A 467 (2013) 483–496)

3.2.3. Internally illuminated monolith reactor

Furthermore, an internally illuminated monolith reactor is successfully designed and assembled to perform photocatalytic CO_2 reduction (Figure 5) [53].
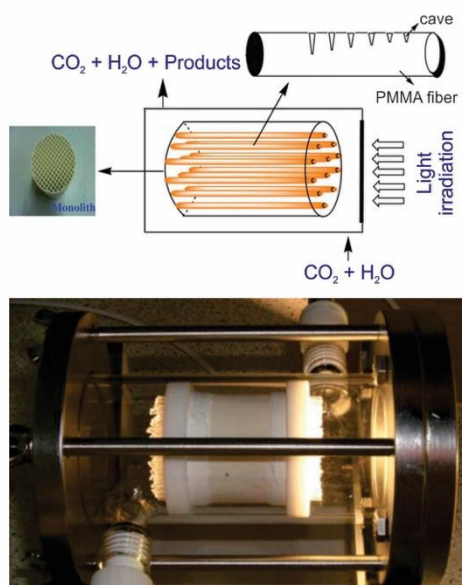
Figure 5. Schematic and digital photograph of an internally illuminated monolith reactor. (Reprinted from P.-Y. Liou et al./ Energy Environ. Sci., 2011, 4, 1487–1494)

A uniform $NiO/InTaO_4$ layer was obtained from the top of a pre-coated SiO_2 sublayer on the internal channels of the monolith. The monolith structure could significantly increase the number of catalysts loaded due to the multiple channels. The carved optical fibers were inserted to transmit and scatter light to illuminate the catalyst inside the monolith channels. Recently, Ola et al. conducted and compared the performance of CO_2 photocatalytic reduction in a slurry batch annular reactor and an internally illuminated monolith reactor [54]. Due to the combined advantages of both the monolith (high surface area) and the optical fibers (uniform light distribution), the quantum efficiency of the internally illuminated monolith reactor was 23.5 times higher than that of the traditional slurry batch annular reactor. A reactor with high quantum efficiency will play an essential role in a commercial scale-up application for producing solar fuels in the future.

3.3. Membrane reactor

Membrane reactor type (twin-reactor) is promoted to combine photocatalytic water-splitting and CO_2 hydrogenation. This design is combined between slurry and fixed-bed reactors (as seen in Fig. 6). There are two major advantages in the membrane reactor. Firstly, CO_2 could be directly hydrogenated to hydrocarbons by the produced H_2. Secondly, the separation of H_2 and O_2 prevents the backward reaction of water splitting and the oxidation of the produced hydrocarbons by O_2 back into CO_2. Applying the membrane reactor could improve both photo-reduction quantum efficiency (PQE) and the selectivity for CO_2 reduction (SCR) [68]. Membrane reactor performs PQE more than four folds from 0.015 % to 0.070 %, compared with the slurry reactor. The SCR in the membrane reactor reaches to 99.1 % which is higher than that in the slurry reactor (73.6 %). Despite the noticeable results achieved, there is a need for further improving the efficiency of photocatalytic CO_2 hydrogenation. The bottleneck is the limited efficiency of the H_2-generating.
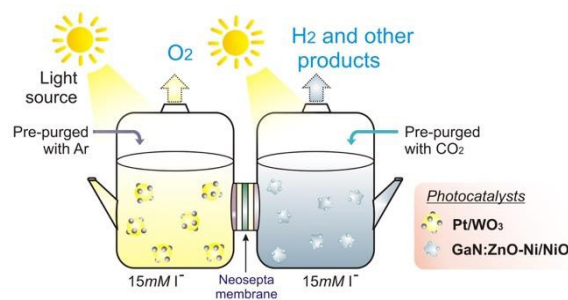

Figure 6. Schematic of the membrane reactor. (Reprinted from Yu et al./ Appl. Catal. A 518 (2016) 158–166)

4. SUMMARY AND FUTURE PERSPECTIVES

In summary, the approach of converting the CO_2 greenhouse gas into renewable fuels using sunlight is considered a viable solution to simultaneously solve global warming and sustainable energy shortage problems. Several photocatalyst materials, reactor types have been designed for photocatalytic conversion of CO_2 to produce solar fuels. Among photocatalysts, salt composites and ZIFs, which are economical materials, have exhibited outstanding photocatalytic efficiencies. It is noted that the optimization of the operating conditions, such as temperature, pressure, and light, plays a vital role in achieving a good yield and product selectivity. Among reactor types, an internally illuminated monolith reactor performs an excellent photocatalytic activity. It showed a 23.5-fold increase in quantum efficiency compared to the traditional slurry reactor. Because low surface-to-volume ratios and inefficient light distribution are the primary concerns during the design of the reactor, additional studies must focus more on (1) improving the geometrical arrangement of the radiation source relative to the reaction space and (2) increasing the illuminated surface area to reactor volume.

From our point of view, photocatalytic conversion of CO_2 is promising and potentially feasible technology that not only convert sunlight energy into solar fuels but also reduce atmospheric CO_2; however, their efficiency is still relatively low and far away from the benchmark photo-conversion efficiency for commercialization. The reason is that photocatalysts and their experimental conditions, such as the nature of the reactors, reaction temperature, pressure, and light source specifications, have not been well optimized. To further enhance the photocatalytic performance, emphases are given to:

(1) Continually develop more efficient photocatalysts with higher mechanical and chemical stabilities and a broader optical absorption band while slowing down the undesirable recombination of e^-/h^+ pairs;

(2) Focus on elucidating mechanisms, surface reaction pathways, electron transfer dynamics, and reaction intermediates through in-situ spectroscopic techniques (XANES, FT-IR, Raman), carbon isotopes (13C-labeled CO_2) supported by theoretical studies to explain the formation of various products;

(3) Systematically develop and explore models simulating the performance of the reactor;

(4) Understand the optical properties and geometrical arrangement of the radiation source relative to the reaction space in different reactor systems.

5. REFERENCES

[1] Gielen D, Boshell F, Saygin D. Climate and energy challenges for materials science. *Nat Mater*. **2016**, 15, 117-20.

[2] Saeidi S, Amin NAS, Rahimpour MR. Hydrogenation of CO2 to value-added products—A review and potential future developments. *J CO2 Util*. **2014**, 5, 66-81.

[3] Aresta M, Dibenedetto A. Industrial utilization of carbon dioxide (CO2). In: Maroto-Valer MM, editor. Developments and Innovation in Carbon Dioxide (CO2) Capture and Storage Technology: Woodhead Publishing, **2010**. 377-410.

[4] Noji T, Jin T, Nango M, Kamiya N, Amao Y. CO2 Photoreduction by Formate Dehydrogenase and a Ru-Complex in a Nanoporous Glass Reactor. *ACS Appl Mater Interfaces*. **2017**.

[5] Kodaka M, Kubota Y. Effect of structures of bipyridinium salts on redox potential and its application to CO2 fixation. *J Chem Soc Perkin Trans 2*. **1999**, 891-4.

[6] Yutaka A, Shusaku I. Discovery of the Reduced Form of Methylviologen Activating Formate Dehydrogenase in the Catalytic Conversion of Carbon Dioxide to Formic Acid. *Chem Lett*. **2015**, 44, 1182-4.

[7] Abe T, Tanizawa M, Watanabe K, Taguchi A. CO2 methanation property of Ru nanoparticle-loaded TiO2 prepared by a polygonal barrel-sputtering method. *Energy Environ Sci*. **2009**, 2, 315-21.

[8] Liu X, Song Y, Geng W, Li H, Xiao L, Wu W. Cu-Mo2C/MCM-41: An Efficient Catalyst for the Selective Synthesis of Methanol from CO2. *Catalysts*. **2016**, 6, 75.

[9] Huang C, Chen S, Fei X, Liu D, Zhang Y. Catalytic Hydrogenation of CO2 to Methanol: Study of Synergistic Effect on Adsorption Properties of CO2 and H2 in CuO/ZnO/ZrO2 System. *Catalysts*. **2015**, 5, 1846.

[10] Kothandaraman J, Goeppert A, Czaun M, Olah GA, Prakash GKS. Conversion of CO2 from Air into Methanol Using a Polyamine and a Homogeneous Ruthenium Catalyst. *J Am Chem Soc* **2016**, 138, 778-81.

[11] Li X, Wang Q, Zhao Y, Wu W, Chen J, Meng H. Green synthesis and photo-catalytic performances for ZnO-reduced graphene oxide nanocomposites. *J Colloid Interface Sci*. **2013**, 411, 69-75.

[12] Cui S-C, Sun X-Z, Liu J-G. Photo-reduction of CO2 Using a Rhenium Complex Covalently Supported on a Graphene/TiO2 Composite. *ChemSusChem*. **2016**, 9, 1698-703.

[13] Nguyen T-V, Wu JCS. Photoreduction of CO2 to fuels under sunlight using optical-fiber reactor. *Sol Energy Mater Sol Cells*. **2008**, 92, 864-72.

[14] Wu H-Y, Bai H, Wu JCS. Photocatalytic Reduction of CO2 Using Ti–MCM-41 Photocatalysts in Monoethanolamine Solution for Methane Production. *Ind Eng Chem Res*. **2014**, 53, 11221-7.

[15] Benson EE, Kubiak CP, Sathrum AJ, Smieja JM. Electrocatalytic and homogeneous approaches to conversion of CO2 to liquid fuels. *Chem Soc Rev*. **2009**, 38, 89-99.

[16] Rezaei B, Mokhtarianpour M, Ensafi AA, Hadadzadeh H, Shakeri J. Electrocatalytic reduction of CO2 using the dinuclear rhenium(I) complex [ReCl(CO)3(μ-tptzH)Re(CO)3]. *Polyhedron*. **2015**, 101, 160-4.

[17] Nguyen V-H, Wu JCS. Recent developments in the design of photoreactors for solar energy conversion from water splitting and CO2 reduction. *Applied Catalysis A: General*. **2018**, 550, 122-41.

[18] Khan AA, Tahir M. Recent advancements in engineering approach towards design of photo-reactors for selective photocatalytic CO2 reduction to renewable fuels. *Journal of CO2 Utilization*. **2019**, 29, 205-39.

[19] Kočí K, Obalová L, Lacný Z. Photocatalytic reduction of CO2 over TiO2 based catalysts. *Chemical Papers*, **2008**, 62.1: 1-9.

[20] Tahir M, Amin NS. Indium-doped TiO2 nanoparticles for photocatalytic CO2 reduction with H2O vapors to CH4. *Appl Catal, B*. **2015**, 162, 98-109.

[21] Ola O, Maroto-Valer MM. Transition metal oxide based TiO2 nanoparticles for visible light induced CO2 photoreduction. *Appl Catal, A*. **2015**, 502, 114-21.

[22] Kong D, Tan JZY, Yang F, Zeng J, Zhang X. Electrodeposited Ag nanoparticles on TiO2 nanorods for enhanced UV visible light photoreduction CO2 to CH4. *Appl Surf Sci*. **2013**, 277, 105-10.

[23] Collado L, Reynal A, Coronado JM, Serrano DP, Durrant JR, de la Peña O'Shea VA. Effect of Au surface plasmon nanoparticles on the selective CO2 photoreduction to CH4. *Appl Catal, B*. **2015**, 178, 177-85.

[24] Phongamwong T, Chareonpanich M, Limtrakul J. Role of chlorophyll in Spirulina on photocatalytic activity of CO2 reduction under visible light over modified N-doped TiO2 photocatalysts. *Appl Catal, B*. **2015**, 168, 114-24.

[25] Ahmad Beigi A, Fatemi S, Salehi Z. Synthesis of nanocomposite CdS/TiO2 and investigation of its photocatalytic activity for CO2 reduction to CO and CH4 under visible light irradiation. *J CO2 Util*. **2014**, 7, 23-9.

[26] Truong QD, Liu J-Y, Chung C-C, Ling Y-C. Photocatalytic reduction of CO2 on FeTiO3/TiO2 photocatalyst. *Catal Commun*. **2012**, 19, 85-9.

[27] Liu L, Zhao C, Pitts D, Zhao H, Li Y. CO2 photoreduction with H2O vapor by porous MgO-TiO2 microspheres: effects of surface MgO dispersion and CO2 adsorption-desorption dynamics. *Catal Sci Technol*. **2014**, 4, 1539-46.

[28] Zhang Z, Huang Z, Cheng X, Wang Q, Chen Y, Dong P, et al. Product selectivity of visible-light photocatalytic reduction of carbon dioxide using titanium dioxide doped by different nitrogen-sources. *Appl Surf Sci*. **2015**, 355, 45-51.

[29] Abdullah H, Khan MMR, Ong HR, Yaakob Z. Modified TiO2 photocatalyst for CO2 photocatalytic reduction: An overview. *J CO2 Util*. **2017**, 22, 15-32.

[30] Low J, Cheng B, Yu J. Surface modification and enhanced photocatalytic CO2 reduction performance of TiO2: a review. *Appl Surf Sci*. **2017**, 392, 658-86.

[31] Nikokavoura A, Trapalis C. Alternative photocatalysts to TiO2 for the photocatalytic reduction of CO2. *Appl Surf Sci*. **2017**, 391, 149-74.

[32] Kumar P, Mungse HP, Cordier S, Boukherroub R, Khatri OP, Jain SL. Hexamolybdenum clusters supported on graphene oxide: Visible-light induced photocatalytic reduction of carbon dioxide into methanol. *Carbon*. **2015**, 94, 91-100.

[33] Yahaya AH, Gondal MA, Hameed A. Selective laser enhanced photocatalytic conversion of CO2 into methanol. *Chem Phys Lett*. **2004**, 400, 206-12.

[34] Lv M, Liu H. Photocatalytic property and structural stability of CuAl-based layered double hydroxides. *J Solid State Chem*. **2015**, 227, 232-8.

[35] Li J, Luo D, Yang C, He S, Chen S, Lin J, et al. Copper(II) imidazolate frameworks as highly efficient photocatalysts for reduction of CO2 into methanol under visible light irradiation. *J Solid State Chem*. **2013**, 203, 154-9.

[36] Jiang W, Yin X, Xin F, Bi Y, Liu Y, Li X. Preparation of CdIn2S4 microspheres and application for photocatalytic reduction of carbon dioxide. *Appl Surf Sci*. **2014**, 288, 138-42.

[37] Yue PL. *Introduction to the Modelling and Design of Photoreactors. In: Schiavello M, editor. Photoelectrochemistry, Photocatalysis and Photoreactors: Fundamentals and Developments*. Dordrecht: Springer Netherlands; **1985**, 527-47.

[38] Cassano AE, Martin CA, Brandi RJ, Alfano OM. Photoreactor Analysis and Design: Fundamentals and Applications. *Ind Eng Chem Res*. **1995**, 34, 2155-201.

[39] Inoue T, Fujishima A, Konishi S, Honda K. Photoelectrocatalytic reduction of carbon dioxide in aqueous suspensions of semiconductor powders. *Nature*. **1979**, 277, 637-8.

[40] Fujiwara H, Hosokawa H, Murakoshi K, Wada Y, Yanagida S. Surface Characteristics of ZnS Nanocrystallites Relating to Their Photocatalysis for CO2 Reduction1. *Langmuir*. **1998**, 14, 5154-9.

[41] Grodkowski J, Neta P. Cobalt Corrin Catalyzed Photoreduction of CO2. *J Phys Chem, A*. **2000**, 104, 1848-53.

[42] Lu D, Zhang M, Zhang Z, Li Q, Wang X, Yang J. Self-organized vanadium and nitrogen co-doped titania nanotube arrays with enhanced photocatalytic reduction of CO2 into CH4. *Nanoscale Res Lett*. **2014**, 9, 272.

[43] Yang H-C, Lin H-Y, Chien Y-S, Wu JC-S, Wu H-H. Mesoporous TiO2/SBA-15, and Cu/TiO2/SBA-15 Composite Photocatalysts for Photoreduction of CO2 to Methanol. *Catal Lett*. **2009**, 131, 381-7.

[44] Wu H-Y, Nguyen NH, Bai H, Chang S-m, Wu JCS. Photocatalytic reduction of CO2 using molybdenum-doped titanate nanotubes in a MEA solution. *RSC Adv*. **2015**, 5, 63142-51.

[45] Yamagata S, Nishijo M, Murao N, Ohta S, Mizoguchi I. CO2 reduction to CH4 with H2 on photoirradiated TS-1. *Zeolites*. **1995**, 15, 490-3.

[46] Zhang Q-H, Han W-D, Hong Y-J, Yu J-G. Photocatalytic reduction of CO2 with H2O on Pt-loaded TiO2 catalyst. *Catal Today*. **2009**, 148, 335-40.

[47] Tan SS, Zou L, Hu E. Photocatalytic reduction of carbon dioxide into gaseous hydrocarbon using TiO2 pellets. *Catal Today*. **2006**, 115, 269-73.

[48] Lo C-C, Hung C-H, Yuan C-S, Wu J-F. Photoreduction of carbon dioxide with H2 and H2O over TiO2 and ZrO2 in a circulated photocatalytic reactor. *Sol Energy Mater Sol Cells*. **2007**, 91, 1765-74.

[49] Chen B-R, Nguyen V-H, Wu JCS, Martin R, Koci K. Production of renewable fuels by the photohydrogenation of CO2: effect of the Cu species loaded onto TiO2 photocatalysts. *Phys Chem Chem Phys*. **2016**, 18, 4942-51.

[50] Nguyen T-V, Wu JCS. Photoreduction of CO2 in an optical-fiber photoreactor: Effects of metals addition and catalyst carrier. *Appl Catal, A*. **2008**, 335, 112-20.

[51] Nguyen T-V, Wu JCS, Chiou C-H. Photoreduction of CO2 over Ruthenium dye-sensitized TiO2-based catalysts under concentrated natural sunlight. *Catal Commun*. **2008**, 9, 2073-6.

[52] Tahir M, Amin NS. Photocatalytic CO2 reduction and kinetic study over In/TiO2 nanoparticles supported microchannel monolith photoreactor. *Appl Catal, A*. **2013**, 467, 483-96.

[53] Liou P-Y, Chen S-C, Wu JCS, Liu D, Mackintosh S, Maroto-Valer M, et al. Photocatalytic CO2 reduction using an internally illuminated monolith photoreactor. *Energy Environ Sci*. **2011**, 4, 1487-94.

[54] Ola O, Maroto-Valer M, Liu D, Mackintosh S, Lee C-W, Wu JCS. Performance comparison of CO2 conversion in slurry and monolith photoreactors using Pd and Rh-TiO2 catalyst under ultraviolet irradiation. *Appl Catal, B*. **2012**, 126, 172-9.

[55] Lee YY, Jung HS, Kim JM, Kang YT. Photocatalytic CO2 conversion on highly ordered mesoporous materials: Comparisons of metal oxides and compound semiconductors. *Applied Catalysis B: Environmental*. **2018**, 224, 594-601.

[56] Chen C-Y, Yu J, Nguyen V-H, Wu J, Wang W-H, Kočí K. Reactor Design for CO2 Photo-Hydrogenation toward Solar Fuels under Ambient Temperature and Pressure. *Catalysts*. **2017**, 7, 63.

[57] Ola O, Maroto-Valer MM. Review of material design and reactor engineering on TiO2 photocatalysis for CO2 reduction. *J Photochem Photobiol, C*. **2015**, 24, 16-42.

[58] Hofstadler K, Bauer R, Novalic S, Heisler G. New Reactor Design for Photocatalytic Wastewater Treatment with TiO2 Immobilized on Fused-Silica Glass Fibers: Photomineralization of 4-Chlorophenol. *Environ Sci Tech*. **1994**, 28, 670-4.

[59] Wang Z-Y, Chou H-C, Wu JCS, Tsai DP, Mul G. CO2 photoreduction using NiO/InTaO4 in optical-fiber reactor for renewable energy. *Appl Catal, A*. **2010**, 380, 172-7.

[60] Wu JS. Photocatalytic Reduction of Greenhouse Gas CO2 to Fuel. *Catal Surv Asia*. **2009**, 13, 30-40.

[61] Wu JCS, Lin H-M, Lai C-L. Photo reduction of CO2 to methanol using optical-fiber photoreactor. *Appl Catal, A*. **2005**, 296, 194-200.

[62] Wu JCS, Wu T-H, Chu T, Huang H, Tsai D. Application of Optical-fiber Photoreactor for CO2 Photocatalytic Reduction. *Top Catal*. **2008**, 47, 131-6.

[63] Usubharatana P, McMartin D, Veawab A, Tontiwachwuthikul P. Photocatalytic Process for CO2 Emission Reduction from Industrial Flue Gas Streams. *Ind Eng Chem Res*. **2006**, 45, 2558-68.

[64] Tahir M, Tahir B. Dynamic photocatalytic reduction of CO2 to CO in a honeycomb monolith reactor loaded with Cu and N doped TiO2 nanocatalysts. *Appl Surf Sci*. **2016**, 377, 244-52.

[65] Tahir M, Amin NS. Photocatalytic CO2 reduction with H2 as reductant over copper and indium co-doped TiO2 nanocatalysts in a monolith photoreactor. *Appl Catal, A*. **2015**, 493, 90-102.

[66] Wu Y-T, Yu Y-H, Nguyen V-H, Lu K-T, Wu JC-S, Chang L-M, et al. Enhanced xylene removal by photocatalytic oxidation using fiber-illuminated honeycomb reactor at ppb level. *J Hazard Mater*. **2013**, 262, 717-25.

[67] Lu K-T, Nguyen V-H, Yu Y-H, Yu C-C, Wu JCS, Chang L-M, et al. An internal-illuminated monolith photoreactor towards efficient photocatalytic degradation of ppb-level isopropyl alcohol. *Chem Eng J*. **2016**, 296, 11-8.

[68] Yu S-H, Chiu C-W, Wu Y-T, Liao C-H, Nguyen V-H, Wu JCS. Photocatalytic water splitting and hydrogenation of CO2 in a novel twin photoreactor with IO3−/I− shuttle redox mediator. *Applied Catalysis A: General*. **2016**, 518, 158-66.

Table 1. *Summary of advantages and disadvantages for catalytic CO_2 reduction processes*

No.	Catalytic process	Advantages	Disadvantages
1	Biocatalytic	+ High efficiency; + None toxicity; + Excellent biodegradability; + Possibility to synthesize liquid fuels	+ Cumbersome process
2	Catalytic (Heterogeneous catalysis)	+ Excellent performance, efficiency; + Easy recyclability	+ High temperature requirement; + Low selectivity
	Catalytic (Homogeneous catalysis)	+ Excellent performance, efficiency; + High selectivity.	+ Separation concern for reaction product; + Not stable toward heat and pressure; + Difficult recyclability.
3	Photocatalytic (Heterogeneous photocatalysis)	+ Artificial photosynthesis for storage of solar energy; + A cost-competitive, safety and eco-friendly alternative toward solar fuels; + Easy recyclability	+ Low efficiency
	Photocatalytic (Homogeneous photocatalysis)	+ Artificial photosynthesis for storage of solar energy; + A cost-competitive, safety and eco-friendly alternative toward solar fuels	+ Separation concern for reaction product; + Difficult recyclability.
4	Electrocatalytic	+ Possibility to directly synthesize liquid fuels (long-chain molecule)	+ High energy barrier

Table 2. *Summary of performance under different modification techniques for TiO_2.*

No.	Modification techniques	Photocatalysts	Reaction Conditions	Products	Yield	Ref.
1	cation doping	TiO_2	Halogen lamp (500W; 380-1100 nm; 68.35 mW·cm^{-2});	CH_3OH	No product formation;	[21]
		V/TiO_2			1.2 μmol·g$_{cat}^{-1}$·h^{-1};	
		Cr/TiO_2			0.7 μmol·g$_{cat}^{-1}$·h^{-1};	
		Co/TiO_2			1.6 μmol·g$_{cat}^{-1}$·h^{-1};	
2		TiO_2	Mercury flash lamp (500W; 365 nm; 40 mW·cm^{-2});	CH_4	36.5 μmol·g$_{cat}^{-1}$·h^{-1};	[20]
		In/TiO_2			578 μmol·g$_{cat}^{-1}$·h^{-1};	
3		TiO_2	Four UV bulbs (8W; 365 nm; 3.25 mW·cm^{-2});	CH_4	0.5 μmol·g$_{cat}^{-1}$·h^{-1};	[22]
		Ag/TiO_2			2.6 μmol·g$_{cat}^{-1}$·h^{-1};	
4		TiO_2	White light LED (30W; 400–455 nm;	CH_4	0.4 μmol·g$_{cat}^{-1}$·h^{-1};	[23]
		Au/TiO_2			4.9 μmol·g$_{cat}^{-1}$·h^{-1};	
5	anion doping	TiO_2	The compact fluorescent integrated bulbs (Philips Tornado: 6 bulbs; 13W; 400-800 nm; 0.37 mW·cm^{-2});	CH_4	0.05 μmol·g$_{cat}^{-1}$·h^{-1};	[24]
		N/TiO_2			0.15 μmol·g$_{cat}^{-1}$·h^{-1};	
6	semiconductors coupling	TiO_2	Mercury lamp (125W; 350-400 nm);	CH_4	No product formation;	[25]
		CdS/TiO_2			0.19 μmol·g$_{cat}^{-1}$·h^{-1};	
7		TiO_2	High-pressure Xe lamp (500W; < 300 nm);	CH_3OH	0.17 μmol·g$_{cat}^{-1}$·h^{-1};	[26]
		$FeTiO_3/TiO_2$			0.47 μmol·g$_{cat}^{-1}$·h^{-1};	
8	surface alkali/ base modification	MgO/TiO_2	Oriel Xe lamp (400W; 200-1000 nm; 420 mW·cm^{-2});	CO	4.0 μmol·g$_{cat}^{-1}$·h^{-1};	[27]
		MgO/TiO_2			37.5 μmol·g$_{cat}^{-1}$·h^{-1};	
		TiO_2	Visible light sources (300W; UV < 5%; 420 mW·cm^{-2});	CH_4	6.9 ppm·g$_{cat}^{-1}$·h^{-1};	[28]
		N_2H_4/TiO_2			416 ppm·g$_{cat}^{-1}$·h^{-1};	
9		NH_3/TiO_2			338 ppm·g$_{cat}^{-1}$·h^{-1};	

Table 3. *Summary of photocatalytic reduction and hydrogenation of CO₂ for producing solar fuels*

No.	Reactor	Photocatalyst	Experiment setup	Light source	Main Products	Ref.
1	A glass cell	TiO_2	Purified water (100 ml) contained 1 g photocatalyst was bubbled by CO_2 gas (3 l·ml⁻¹).	High-pressure Hg arc lamp (500 W)	HCHO: 1.6×10^{-4} M·h⁻¹; CH$_3$OH: 3.3×10^{-5} M·h⁻¹;	[39]
2		ZnO			HCHO: 1.7×10^{-4} M·h⁻¹; CH$_3$OH: 0.5×10^{-4} M·h⁻¹;	
3		CdS			HCHO: 2.9×10^{-4} M·h⁻¹; CH$_3$OH: 1.7×10^{-4} M·h⁻¹;	
4		GaP			HCHO: 1.4×10^{-4} M·h⁻¹; CH$_3$OH: 1.6×10^{-4} M·h⁻¹;	
5		SiC			HCHO: 1.4×10^{-4} M·h⁻¹; CH$_3$OH: 7.6×10^{-4} M·h⁻¹;	
6	A closed pyrex tube	ZnS	A DMF solution (2 mL) containing 10mM (diatomic) of ZnS nanocrystallites and 1 M of distilled triethylamine (TEA) was saturated with CO_2 for photo-redox reactions.	A high-pressure Hg lamp (500 W; $\lambda > 290$ nm)	CO: 12.4 µmol·h⁻¹; HCOO⁻: 9.4 µmol·h⁻¹; H$_2$: 7.4 µmol·h⁻¹;	[40]
7	A pyrex bulb	CoTTP	An acetonitrile/methanol (9/1 v/v) solutions containing p-terphenyl (TP, 3 mmol·l⁻¹) as a photosensitizer, trimethylamine (TEA, 5 %) as a reductive quencher, and 0.05 mmol·l⁻¹ Co complex.	Xe lamp	CO: 0.41 mmol·l⁻¹; H$_2$: 0.92 mmol·l⁻¹;	[41]
8		hydroxocobalamin			CO: 2.25 mmol·l⁻¹; H$_2$: 3.44 mmol·l⁻¹;	
9	A cylindrical glass vessel	V, N co-doped TiO_2 nanotube arrays (TNAs)	TNAs films were placed in the center before sealing the reactor contained 20 ml 0.1 mol·l⁻¹ KHCO$_3$ solution.	Hg lamp (300 W)	CH$_4$: 64.5 ppm·cm⁻²·h⁻¹;	[42]
10	A stirred batch annular quartz reactor	TiO_2/SBA-15	550 ml aqueous 0.1 N NaOH solution containing about 0.05 g catalyst at 315 K. CO_2 gas was bubbled into the reactor continuously, and the pH value was kept near pH 7 during the reaction.	Medium-pressure metal halide lamp (400 W, Phillps HPA400, 365 nm)	CH$_3$OH: 627 µmol·g⁻¹·h⁻¹;	[43]
11		Cu/TiO_2/SBA-15			CH$_3$OH: 690 µmol·g⁻¹·h⁻¹;	
12	A slurry batch reactor	Mo-doped TNTs (Mo-T-500)	Photocatalyst (0.1 g) was loaded in 300 ml of 0.2 M MEA solution contained 0.1 g at the saturated absorption of CO_2. The reaction temperature was controlled at 298±2 K.	UVC lamp (8 W; 365 nm; 63 W·cm⁻²)	CH$_4$: 0.52 µmol·g$_{cat}$⁻¹; CO: 10.41 µmol·g$_{cat}$⁻¹; PQE: 0.22 %.	[44]
13	A closed circulation gas reactor	TS-1	The prior reaction, photocatalyst (20 mg) was activated by UV irradiation under an H$_2$ atmosphere (1.0×10^5 Pa). After H$_2$ was evacuated, reactant gas was introduced (1.0×10^5 Pa).	Hg lamp (Ushio ML-251 A/A)	CH$_4$: 7.8×10^{-8} mol·h⁻¹;	[45]
14	A fixed-bed reactor	Pt/ TiO_2 nanotube	The reaction was carried out with catalysts (50 mg), CO_2 (99.5% purity) and H$_2$O vapor. The amount of H$_2$O vapor depended on the H$_2$O/CO_2 molar ratio, which was regulated by the temperature in the conical flask.	High-pressure Hg lamp (300 W, 365 nm)	CH$_4$: 4.8 µmol·g$_{Ti}$⁻¹·h⁻¹;	[46]
15		Pt/ TiO_2 (P25)			CH$_4$: 3.9 µmol·g$_{Ti}$⁻¹·h⁻¹;	
16	A fixed-bed reactor	TiO_2 pellets: JRC-TiO-4	TiO_2 pellets (100 g) was spread out on the flat tray in the reactor.	NEC Germicidal	CH$_4$: 1.4×10^{-2} µmol·g$_{cat}$⁻¹·h⁻¹;	[47]

17		TiO_2 pellets: porous Vycor glass (PVG)	The reactants included water (vapor) and highly purified (99.999%) CO_2 gas.	lamps (1.6 W; GL8; 253.7 nm)	CH_4: 2.5×10^{-3} $\mu mol \cdot g_{cat}^{-1} \cdot h^{-1}$;	
18		TiO_2 pellets: Aerolyst 7708			CH_4: 2.1×10^{-3} $\mu mol \cdot g_{cat}^{-1} \cdot h^{-1}$;	
19	A circulated reactor	TiO_2 immobilized Pyrex glass pellets	+ CO_2 (99.8 %, SUPELCO Scott Specialty Gases, Cat. No. 501298): 5 %; + H_2 (99.995 %): 90 %; + H_2O (D.I. water): 5 %;	A near-UV fluorescent black lamp (4×15 W; Sankyo Denki Co. Ltd., Japan; F10TBLB; 365 nm)	CH_4: 4.11 $mmol \cdot g_{cat}^{-1} \cdot h^{-1}$; CO: 0.14 $mmol \cdot g_{cat}^{-1} \cdot h^{-1}$; C_2H_6: 0.10 $mmol \cdot g_{cat}^{-1} \cdot h^{-1}$;	[48]
20	A single pyrex reactor	Cu/TiO_2	H_2O (5 mL), H_2 (0.01 atm), saturated CO_2 (1 atm); 363 K	11SC-1 pen-ray lamp (12 mW cm^{-2}; 254 nm)	CO: 0.54 $\mu mol \cdot g_{cat}^{-1} \cdot h^{-1}$; CH_4: 3.59 $\mu mol \cdot g_{cat}^{-1} \cdot h^{-1}$; PQE: 0.13 %;	[49]
21			H_2O (5 mL), saturated CO_2 (1 atm)		CO: 0.03 $\mu mol \cdot g_{cat}^{-1} \cdot h^{-1}$; CH_4: 0.67 $\mu mol \cdot g_{cat}^{-1} \cdot h^{-1}$; PQE: 0.03 %;	
22	An optical-fiber reactor	Cu(0.5 wt%)-Fe(0.5 wt%)/ TiO_2/ glass plate	The reactor was purged by CO_2 gas bubbling through D.I. water for 1 h at 348 K. The space velocity of the CO_2 gas and H_2O vapor was maintained at 0.72 h^{-1}.	High pressure Hg lamp (150 W; 225 mW·cm^{-2}; 320–500 nm)	C_2H_4: 0.05 $\mu mol \cdot g_{cat}^{-1} \cdot h^{-1}$; CH_4: 0.06 $\mu mol \cdot g_{cat}^{-1} \cdot h^{-1}$;	[50]
23		Cu(0.5 wt%)-Fe(0.5 wt%)/ TiO_2/ optical fiber			C_2H_4: 0.05 $\mu mol \cdot g_{cat}^{-1} \cdot h^{-1}$; CH_4: 0.06 $\mu mol \cdot g_{cat}^{-1} \cdot h^{-1}$;	
24	An optical-fiber reactor	N3-dye-Cu(0.5 wt%)-Fe(0.5 wt%)/TiO_2	The reactor was purged by CO_2 gas bubbling through D.I. water for 1 h at 348 K. The space velocity of the CO_2 gas and H_2O vapour was maintained at 0.72 h^{-1}.	Concentrated natural sunlight (20 mW·cm^{-2})	CH_4: 0.62 $\mu mol \cdot g_{cat}^{-1} \cdot h^{-1}$;	[51]
25	A monolith reactor	TiO_2-cell	P_{CO2}= 0.040 bar, P_{H2O} = 0.074 bar, T = 373 K.	Hg lamp (200W; 150 mW·cm^{-2}; 252 nm)	CO: 5.20 $\mu mol \cdot g_{cat}^{-1} \cdot h^{-1}$; CH_4: 7.70 $\mu mol \cdot g_{cat}^{-1} \cdot h^{-1}$; C_2H_4: 0.79 $\mu mol \cdot g_{cat}^{-1} \cdot h^{-1}$;	[52]
26		TiO_2-monolith			CO: 43.00 $\mu mol \cdot g_{cat}^{-1} \cdot h^{-1}$; CH_4: 78.00 $\mu mol \cdot g_{cat}^{-1} \cdot h^{-1}$; C_2H_4: 1.50 $\mu mol \cdot g_{cat}^{-1} \cdot h^{-1}$; C_2H_6: 0.79 $\mu mol \cdot g_{cat}^{-1} \cdot h^{-1}$;	
27		In/TiO_2-monolith			CO: 962.00 $\mu mol \cdot g_{cat}^{-1} \cdot h^{-1}$; CH_4: 55.40 $\mu mol \cdot g_{cat}^{-1} \cdot h^{-1}$; C_2H_4: 0.34 $\mu mol \cdot g_{cat}^{-1} \cdot h^{-1}$; C_2H_6: 1.50 $\mu mol \cdot g_{cat}^{-1} \cdot h^{-1}$; C_3H_6: 0.07 $\mu mol \cdot g_{cat}^{-1} \cdot h^{-1}$;	
28	An internally illuminated monolith reactor	$1\%NiO/InTaO_4$ (sg)	Vapor-phase CO_2 with saturated H_2O was photo-reduced to hydrocarbons by UV or visible-light in a steady-state flow.	Xenon lamp, visible light 42.46 mW·cm^{-2}	CH_3OH: 0.16 $\mu mol \cdot g_{cat}^{-1} \cdot h^{-1}$; QE: 0.012 %;	[53]
29		$1\%NiO/InTaO_4$ (sg)		Mercury lamp, UVA light 42.46 mW·cm^{-2}	C_2H_4O: 0.3 $\mu mol \cdot g_{cat}^{-1} \cdot h^{-1}$; QE: 0.057 %;	
30		$2.6\%NiO/InTaO_4$ (imp)		Xenon lamp, AM1.5G 100 mW·cm^{-2}	C_2H_4O: 0.3 $\mu mol \cdot g_{cat}^{-1} \cdot h^{-1}$; QE: 0.058 %;	
31	A slurry batch	1 wt% Pd/0.01 wt% Rh-TiO_2	200 ml of D.I. water contained 1 g photocatalyst was magnetically stirred at 240 rpm. Ultra-pure	UVA lamp (2×8 W; Sylvania; 3.22	CH_4: 0.03 $\mu mol \cdot g_{cat}^{-1} \cdot h^{-1}$; QE: 0.002 %;	[54]

	annular reactor		CO₂ (Air Products, 99.999%) gas was bubbled at 1 bar for 35 min then the CO₂ supply was cut off.	mW·cm⁻²; 365 nm)	
32	An internally illuminated monolith reactor		The reactor was then purged with He for 1 h, then switched to CO₂ gas saturated with H₂O vapor for 1 h at a flow rate of 4 ml/min. The retention time (volume/flow rate) of the monolith was 54 min. The flow of CO₂ saturated with water vapor was continuous throughout the reaction.	High pressure Hg lamp (Exfo Omnicure S1500; 41.62 mW·cm⁻²; 320–500 nm;	CH₃OH: 0.10 μmol·g$_{cat}$⁻¹·h⁻¹; C₂H₄O: 0.21 μmol·g$_{cat}$⁻¹·h⁻¹; QE: 0.062 %;